Loss of *Prm1* leads to defective chromatin protamination, impaired PRM2 processing, reduced sperm motility and subfertility in male mice

Gina Esther Merges[1], Julia Meier[1], Simon Schneider[1], Alexander Kruse[2], Andreas Christian Fröbius[2], Klaus Steger[2], Lena Arévalo[1] and Hubert Schorle[1]

[1] Department of Developmental Pathology, Institute of Pathology, University Hospital Bonn, Bonn, Germany.

[2] Department of Urology, Pediatric Urology and Andrology, Section Molecular Andrology, Biomedical Research Center of the Justus-Liebig University, Giessen, Germany

Keywords

Protamine ratio, chromatin condensation, spermiogenesis, protamine 1 (*Prm1*), PRM2 processing, infertility, subfertility

Corresponding author: schorle@uni-bonn.de

Abstract

One of the key events during spermiogenesis is the hypercondensation of chromatin by substitution of the majority of histones by protamines. In humans and mice, protamine 1 (*PRM1/Prm1*) and protamine 2 (*PRM2/Prm2*), are expressed in a species-specific ratio. Using CRISPR-Cas9-mediated gene editing we generated *Prm1*-deficient mice and demonstrate, that *Prm1+/-* mice are subfertile while *Prm1-/-* are infertile. *Prm1*-deficiency was associated with higher levels of 8-OHdG, an indicator for reactive oxygen mediated DNA-damage. While *Prm1+/-* males displayed moderate increased levels of 8-OHdG virtually

all sperm of *Prm1-/-* males displayed ROS mediated DNA damage. Consequently, DNA integrity was slightly hampered in *Prm1+/-*, while DNA was completely fragmented in *Prm1-/-* animals. Interestingly CMA3 staining which indicates protamine-free DNA revealed, that *Prm1+/-* sperm displayed high levels (93%), compared to *Prm2+/-* (29%) and WT (2%) sperm. This is not due to increased histone retention as demonstrated by mass spectrometry (MassSpec) of nuclear proteins in *Prm1+/-* sperm. Further analysis of the MassSpec data from sperm nuclear proteome revealed, that only one protein (RPL31) is significantly higher abundant in *Prm1+/-* compared to WT sperm. Comparison of the proteome from *Prm1-/-* and *Prm2-/-* to WT suggested, that there are a small number of proteins which differ in abundance. However, their function was not linked mechanistically to primary defects seen in *Prm1-/-* mice and rather represent a general stress response. Interestingly, using acid urea gels we found that sperm from *Prm1+/-* and *Prm1-/-* mice contain a high level of unprocessed, full-length PRM2. *Prm2* is transcribed as a precursor protein which, upon binding to DNA is successively processed. Further, the overall ratio of PRM1:PRM2 is skewed from 1:2 in WT to 1:5 in *Prm1+/-* animals. Our results reveal that *Prm1* is required for proper processing of PRM2 to produce the mature PRM2 which, together with *Prm1* is able to hypercondense DNA. Hence, the species specific PRM1:PRM2 ratio has to be precisely controlled in order to retain full fertility.

Introduction

During spermatogenesis in the seminiferous epithelium of the testis diploid spermatogonia differentiate into haploid spermatids. One of the most remarkable changes during spermiogenesis is complete reorganization of chromatin compaction [1], where histones are nearly completely substituted by protamines. These are highly basic, arginine rich proteins [2] which, upon binding to DNA hypercondense chromatin, leading to transcriptional silencing and protection of the paternal genome [3]. While in most mammals, DNA compaction in

sperm is accomplished by incorporation of protamine 1 (PRM1) alone, primates and most rodents express two protamines, PRM1 and protamine 2 (PRM2) [4, 5]. In mice and men, *Prm1* and *Prm2* are encoded in a tightly regulated gene cluster on chromosome 16 [6, 7]. While PRM1 is expressed as mature protein, PRM2 is expressed as precursor protein (pre-PRM2), consisting of a C-terminal mature PRM2 (mPRM2) domain and a N-terminal cleaved PRM2 (cPRM2) domain, which is sequentially cleaved off upon binding to DNA [5, 8, 9]. Of note, *mPrm2* is proposed to originate from a gene duplication of *Prm1* [10]. In an evolutionary context *Prm1* and *cPrm2* were shown to be conserved, suggesting important roles in fertility [11, 12]. *PRM1*/PRM1 and *PRM2*/PRM2 are detected in a species-specific ratio (humans 1:1 ([13]), mice 1:2 [14]). In humans, alterations of the protamine ratio (PRM1:PRM2) have been associated with male sub- and infertility [15-27].

Mice chimeric for a deletion of one allele of *Prm1* or *Prm2* [28-30] were infertile and did not allow for the establishment of mouse lines and detailed analysis of *Prm*-deficiency. Further, heterozygous *Prm1*-deficient mice generated with CRISPR-Cas9 have been reported to be infertile [31]. Hence, a detailed phenotypical analysis of *Prm1*-deficient mice was not possible so far.

Schneider *et al.* reported the establishment of *Prm2*-deficient mouse lines using CRISPR-Cas9-mediated gene editing in zygotes [32]. Here, *Prm2+/-* male mice remained fertile while *Prm2-/-* were infertile. While *Prm2+/-* sperm showed no pathomorphological effects, *Prm2-/-* sperm presented with fragmented DNA, disrupted sperm membranes and complete immotility. These defects were shown to accumulate during epididymal transit. It was demonstrated that the *Prm2-/-* mice display a deregulation of proteins leading to an accumulation of reactive oxygen species (ROS) explaining the phenotype observed [33].

Using CRISPR-Cas9-mediated gene-editing in zygotes, we generated mice deficient for *Prm1*. Male mice heterozygous for the mutation (*Prm1+/-*) are subfertile, while *Prm1*-deficient (*Prm1-/-*) males are sterile. Molecular analyses revealed that loss of one allele of *Prm1* leads to a moderate fragmentation of DNA, while in *Prm1-/-* mice complete DNA fragmentation can be observed. Sperm of *Prm1+/-* mice display reduced motility as well as enhanced 8-OHdG

levels indicative of upregulated ROS levels. Most importantly, analyses of sperm nuclear proteins revealed that the processing of PRM2 to its mPRM2 form seems disturbed in *Prm1+/-* animals already. Further, the species-specific protamine ratio is shifted in *Prm1+/-* mice. These data strongly suggest that the species-specific level of PRM1 is required for proper sperm function.

Material and Methods

Ethics statement

All animal experiments were conducted according to the German law of animal protection and in agreement with the approval of the local institutional animal care committees (Landesamt für Natur, Umwelt und Verbraucherschutz, North Rhine-Westphalia, approval ID: AZ84-02.04.2013.A429; AZ81-0204.2018.A369).

Generation of Prm1-deficient mice

Single guide RNAs (sg1_ts: 5´-CACCGCGAAGATGTCGCAGACGG; sg1_bs: 5´-AAACCCGTCTGCGACATCTTCGC; sg2_ts: 5´-CACCGTGTATGAGCGGCGGCGA, sg2_bs: 5´-AAACTCGCCGCCGCTCATACAC) were tested in ES cells as described before [32]. Guides targeted exon 1 and exon 2 of *Prm1.*

CRISPR-Cas9-mediated gene editing of zygotes was performed as described before [32]. In brief, 6-8 weeks old B6D2F1 females were superovulated by intraperitoneal injections of 5 i.u. pregnant mare´s serum (PMS) and 5 i.u. human chorionic gonadotropin (hCG). Females were mated with B6D2F1 males and zygotes were isolated 0.5 dpc. Single guide RNAs (50 ng/µl each) were microinjected together with Cas9 mRNA (100 ng/µl). After culturing in KSOM medium for three days, developing blastocysts were transferred into the uteri of pseudo-pregnant CB6F1 foster mice. Offspring was genotyped by PCR and sequenced to identify founder animals. After first backcrossing to C57BL/6J mice, the F1 generation was

sequenced. The allele (NM_013637.5:c.51_125del) was further back-crossed to C57BL/6J mice. Starting from the N3 generation analyses were performed, using male mice aged between 8-13 weeks.

Prm2-deficient mice

Prm2-deficient mice (MGI: 5760133; 5770554) generated and analyzed by Schneider *et al.* [32, 33] were used for comparison.

Genotyping and sequencing of mice

Primers flanking the gene edited region (Prm1_fwd: 5´- CCACAGCCCACAAAATTCCAC, Prm1_rev: 5´- TCGGACGGTGGCATTTTTCA) were used to amplify both the WT and edited allele (Cycling conditions: 2 min 95°C; 30x (30 sec 95°C; 30 sec 64°C; 35 sec 72°C); 5 min 72°C). PCR products (WT allele: 437 bp, *Prm1*⊿167: 270 bp) were separated on agarose gels.

PCR products were cloned using the TOPO™ TA Cloning™ Kit with pCR™2.1- TOPO™ (Thermo Fisher) according to the manufacturer's instructions. Plasmids were transformed into E.cloni ® 10G Chemically Competent Cells (Lucigen, Middleton, WI, USA) according to the manufacturer's instructions, isolated by alkaline lysis and sequenced by GATC/Eurofins (Cologne, Germany).

Fertility assessment

Fertility was tested by mating male mice 1:1/1:2 to C57BL/6J females. Females were examined for presence of a vaginal plug daily. Plug positive females were separated and monitored. Pregnancies and litter sizes were recorded. A minimum of five plugs per male were evaluated.

Immunohistochemistry (IHC)/ Immunofluorescence (IF)

Tissues were fixed in Bouin´s solution or paraformaldehyde (PFA) (4°C, overnight) processed in paraffin and 3 µm sections were generated. After deparaffinization, slides were treated with decondensation buffer, as described [33]. Heat mediated antigen retrieval was performed (citrate buffer pH 6.0) for 20 min, followed by blocking in Tris-HCl buffer (pH 7.4, 5% Bovine serum albumin, 0.5% Triton X-100) and primary antibody treatment overnight at 4°C. For IHC staining against protamines (anti-PRM1 (Hup1N) and anti-PRM2 (Hup2B) Briar Patch Biosciences, Livermore, CA, USA; 1:200), slides were treated with 3 % H_2O_2 for 30 min after decondensation. Biotinylated goat-anti-mouse (Dako, Glostrup, Denmark; E0433; 1:200) was used as secondary antibody (1 h, RT), processed using Vectastain Elite ABC-HRP Kit (Vector Laboratories, Burlingame, CA, USA; PK-6100) and stained with AEC-solution (Dako, AEC+ Substrate, K3469). Counterstain was performed using hematoxylin. For IF against 8-OHdG (Santa Cruz Biotechnology, Dallas, TX, USA; sc-66036; 1:200), goat-anti-mouse Alexa Fluor 488 (Thermo Fisher; A-11001; 1:500) was used as secondary antibody for 2 h at room temperature. Nuclei were stained using 1 µg/ml Hoechst (Thermo Fisher; 33342). 8-OHdG positive sperm were quantified using the Photoshop® counting tool. Two tubuli cross-sections per organ per mouse for three animals per genotype were analyzed.

Macroscopic analysis of testis

Sections of Bouin-fixed testis were deparaffinized, hydrated, stained with Hemalum solution acid (Mayer) and Eosin Y solution (Carl Roth, Karlsruhe, Germany), dehydrated and mounted with Entellan® (Sigma-Aldrich/Merck, Darmstadt, Germany). Tubule diameters were determined measuring the horizontal and vertical diameters of at least 25 tubuli per testis cross-section. The number of elongated spermatids per tubules for a minimum of 5 tubules per mouse was counted with the ImageJ cell counter.

Periodic Acid Schiff (PAS) Staining

PAS staining was performed as described [33]. After deparaffinization and re-hydration slides were incubated for 10 min in periodic acid (0.5%), rinsed in H_2O, incubated 20 min with Schiff reagent, counterstained and mounted.

Isolation of epididymal sperm

Sperm were isolated from the cauda epididymis by swim-out as described [32]. The epididymal tissue was incised multiple times and incubated in M2 medium (Sigma) or PBS at 37°C for 15-30 min.

Transmission electron microscopy

Isolated sperm were pelleted (10,000 g, 2 min), fixed in 3% glutaraldehyde at 4°C overnight, washed with 0.1 M cacodylate buffer (2x 15 min), post-fixed with 2 % osmium tetroxide at 4°C for 2 h and again washed. After dehydration in an ascending ethanol series and contrasting in 70% (v/v) ethanol 0.5% (m/v) uranyl acetate (1 – 1.5 h, 4°C), samples were washed with propylenoxide (3x 10 min, RT) and stored in propylenoxide:Epon C (1:1, (v/v)) at 4°C overnight. Next, the pellets were embedded in Epon C (70 °C, 48 h). Ultra-thin sections were examined with transmission electron microscope CM10 equipped with analySiS imaging software. Using ImageJ, 100 sperm per sample were analyzed to determine the difference between the minimum and maximum grey value. Chromatin condensation status was categorized according to high (<150), intermediate (150-180) and low (>180) difference in grey scale.

Assessment of sperm DNA integrity

Sperm genomic DNA was isolated as described [34] with minor adjustments. Briefly, sperm were incubated in 500 µl lysis buffer (1 M Tris-HCl pH 8.0, 3 M NaCl, 0.5 M EDTA, 20% (m/v) SDS) supplemented with 21 µl 1 M DTT, 2.5 µl 0.5% Triton-X100 and 40 µl 10 mg/ml proteinase K at 50°C overnight. After centrifugation (15,500 x g, 10 min), 1 µl 20 mg/ml glycogen and 1/10 vol 3 M NaAc were added to the supernatant. Precipitation was performed

using absolute ethanol for 2 h at -80°C followed by 45 min at -20°C. The pellet was washed with 75% EtOH and dried in a Speed Vac DNA110 (Savant, Farmingdale, USA). DNA was dissolved in 30 µl TE buffer.

Chromomycin A3 (CMA3) staining

Epididymal sperm were fixed in Carnoys solution (3:1 methanol:acetic acid, (v/v)), spread on microscopic slides and covered with 100 µl CMA3 solution (0.25 mg/ml CMA3 in McIlvaine buffer (pH 7.0, containing 10 mM $MgCl_2$)). After incubation for 20 min in the dark, slides were rinsed with McIlvaine buffer and mounted with ROTI®Mount FluorCare DAPI (Carl Roth, Germany). 400 sperm per mouse were analyzed.

Analysis of sperm membrane integrity

Eosin-Nigrosin staining

50 µl of sperm swim-out and 50 µl Eosin-Nigrosin stain (0.67 g eosin Y (color index 45380), 0.9 g sodium chloride, 10 g nigrosin (color index 50420), 100 ml ddH_2O) were mixed and incubated for 30 sec. 30 µl of the mix was pipetted onto microscope slides, smeared and mounted with Entellan® (Merck, Darmstadt, Germany). 200 sperm per animal were analyzed.

Hypoosmotic swelling test

100 µl of sperm swim-out was mixed with 1 ml pre-warmed HOS solution (1.375 g D-fructose, 0.75 g sodium citrate dihydrate, 100 ml ddH_2O) and incubated for 30 min at 37°C. The solution was dropped onto a microscopic slide, covered with a cover slip and analyzed within 1 h. 200 sperm per animal were evaluated.

RNA sequencing (RNAseq) and differential expression analysis

RNA was extracted from whole testis of three individuals per genotype. After removal of the tunica albuginea, testes were homogenized in TRIzol™ and processed according to the manufacturers protocol (Thermo Fisher). RNA integrity (RIN) was determined using the RNA

Nano 6000 Assay Kit with the Agilent Bioanalyzer 2100 system (Agilent Technologies, Santa Clara, CA, USA). RIN values were > 7 for all samples. RNA sample quality control, library preparation (QuantSeq 3'-mRNA Library Prep (Lexogen, Greenland, NH, USA)) and RNAseq were performed by the University of Bonn Core facility for Next Generation Sequencing (NGS). Sequencing was performed on the Illumina HiSeq 2500 V4 platform, producing >10 million, 50bp 3'-end reads per sample.

Samples were mapped to the mouse genome (GRCm38.89) using HISAT2 2.1 [35] and transcripts were quantified and annotated using StringTie 1.3.3 [36]. Gene annotation was retrieved from the Ensembl FTP server (ftp://ftp.ensembl.org)(GRCm38.89). The python script (preDE.py) included in the StringTie package was used to prepare DEseq2-compatible gene-level count matrices for analysis of differential gene expression. Mapping to the *Prm1* genomic location was visualized using the Integrative Genomics Viewer (IGV) [37].

Differential expression was analyzed using DESeq2 1.16.1 [38]. The adjusted p-value (Benjamini-Hochberg method) cutoff for DE was set at < 0.05, log2 fold change of expression (LFC) cutoff was set at > 1. We performed GO term and pathway overrepresentation analyses on relevant lists of genes using the PANTHER gene list analysis tool with Fisher's exact test and FDR correction [39].

Mass spectrometry and differential protein abundance analysis

Sperm basic nuclear proteins from three WT, *Prm1-/-* and *Prm2-/-* mice were isolated as described below and used for mass spectrometric analysis. Peptide preparation, LC-MS and differential abundance (DA) analysis were performed at the University of Bonn Core facility Mass Spectrometry.

Peptide preparation: Protein solutions (5.5 M urea, 20% 2-mercaptoethanol, 5% acetic acid) were dried in a vacuum concentrator and subjected to in solution preparation of peptides as described previously [40]. Briefly, cysteines were alkylated with acrylamide and digested with trypsin, followed by desalting.

LC-MS measurements were performed according to Arévalo *et al*. [40]. Briefly, peptides were separated on a self-packed reversed-phase column within a 90 min gradient. Peptide ions were analyzed with an Orbitrap Lumos mass spectrometer in data-dependent mode with a top-speed method. Precursors and fragment ions were recorded with the Orbitrap detector.

Raw data processing and was performed with Proteome Discoverer software in combination with Mascot server version 2.6.1 using *Mus musculus* sequences from SwissProt (2021/03, including isoforms), and contaminants (cRAP, [41]). Mascot results were filtered for 1% FDR on the basis of q-values from the percolator algorithm [42]. Spectra with identifications below 1% q-value were sent to a second round of database search with semi-tryptic enzyme specificity Summed abundances were used for relative quantification.

Differential abundance (DA) analysis: DA analysis was performeds using the Bioconductor package proDA [43] using peptide spectrum matches (PSM) level data extracted from Protein Discoverer. Only proteins detected in all genotypes and all replicates with more than two peptides were included in the analysis. The data were log2 transformed and median normalized prior to DA analysis to ensure comparability. The proDA package is based on linear models and utilized Bayesian priors to increase power for differential abundance detection [43]. Proteins with a log2 fold change (LFC) of >1 and false discovery rate adjusted p-value (FDR) <0.05 were considered differentially abundant compared to the WT. Plots were generated using the R-package ggplot2 [44].

Sperm nuclear morphology analysis

Epididymal sperm were analyzed using the ImageJ plugin "Nuclear_Morphology_Analysis_1.18.1_standalone" [45] as described previously [33]. In brief, sperm were fixed in Carnoys solution (3:1 methanol: acetic acid (v/v)), spread on slides, mounted with ROTI®Mount FluorCare DAPI (Carl Roth, Karlsruhe, Germany) and imaged at 100-fold magnification. A minimum of 100 sperm heads per sample from four biological replicates were analyzed.

Sperm motility analysis

Epididymal sperm swim out was performed in 1 ml sterile filtered THY medium (138 mM NaCl, 4.8 mM KCl, 2 mM $CaCl_2$, 1.2 mM KH_2PO_4, 1 mM $MgSO_4$, 5.6 mM glucose, 10 mM HEPES,
0.5 mM sodium pyruvate, 10 mM L-lactate, pH 7.4, 310-320 mOsm) for 15 min at 37°C. Next, sperm were diluted 1:20 – 1:50 in dilution medium (3 mg/ml BSA in THY medium). 30 µl of dilution were pipetted onto a glass slide equipped with a spacer and cover slip, placed on a heated slide holder (37°C) and analyzed under an inverted microscope (Leica, Wetzlar, Germany) equipped with a camera (acA1920-155ucMED; Basler AG, Ahrensburg, Germany). The movement of sperm was recorded at 100 frames/sec for 3 sec and analyzed in ImageJ. The produced "z project" was used to distinguish and count moving and non-moving sperm (n = 100 sperm/ mouse).

Analysis of sperm basic nuclear proteins

Isolation of sperm nuclear proteins was performed according to Soler-Ventura *et al.* [46]. Briefly, sperm were counted, washed in PBS, pelleted and resuspended in 200 µl buffer containing 4 µl 1 M Tris pH8, 0.8 µl 0.5 M $MgCl_2$ and 5 µl Triton X-100. After centrifugation the pellet was mixed with 1 mM PMSF. Lysed cells were mixed with solutions containing PMSF, EDTA, DTT, GuHCl and vinylpyridine and incubated for 30 min at 37°C. Addition of EtOH precipitates DNA. Proteins are dissolved in 0.5 M HCl and precipitated with TCA. After acetone washes the proteins are lyophilized and resuspended in sample buffer (5.5 M Urea, 20% 2-mercaptoethanol, 5% acetic acid).
Next, the nuclear proteins were separated on a pre-electrophorized 15% acid-urea polyacrylamide gel (2.5 M urea, 0.9 M acetic acid, and 15% acrylamide/ 0.1% N,N′-Methylene bis-acrylamide, TEMED and APS) and visualized with Coomassie Brilliant Blue. Quantification was performed utilizing ImageJ as described previously [40].

Statistics

Values are, if not indicated otherwise, presented as mean values with standard deviation. Statistical significance was calculated by two-tailed, unpaired Student's t-test and a value of $p < 0.05$ was considered significant ($p < 0.05$= *; $p < 0.005$= **; $p < 0.001$= ***).

Results

CRISPR-Cas9-mediated gene editing produces Prm1-deficient mice

Prm1-deficient mice were generated using CRISPR-Cas9-mediated gene editing. Guide RNAs targeting exon 1 and exon 2 of *Prm1* and Cas9 mRNA were injected into zygotes. From the 13 pups obtained four contained a deletion in the *Prm1* coding region. Those animals were mated to C57BL/6J mice and from the offspring the *Prm1* locus was sequenced. We selected a mouse carrying a 167 bp in frame deletion in the *Prm1* coding region (**Fig. 1a**) and established a PCR-based genotyping (**Fig. 1b**).

In order to validate the deletion, 3´-mRNA sequencing of whole testis of WT (*Prm1*+/+) and *Prm1*-/- males was performed. In *Prm1*-/- males the transcripts mapped to the 5´ and the 3´and ends of the *Prm1* locus while we could not detect transcripts from the central, deleted area, which encodes for crucial arginine sites required for DNA binding (**Fig. 1a, Supplementary Fig. 1**).

Next, we used immunohistochemical (IHC) staining with an anti-PRM1 antibody, targeting an epitope at the N-terminus of PRM1 (marked in red (**Fig. 1a**)) in order to determine, whether the potential transcripts of the gene-edited allele result in the production of a truncated PRM1 protein. However, we could not detect a signal in testis sections of *Prm1*-/- males (**Fig. 1c**). This strongly suggests nonsense mediated RNA decay of the potential transcript and demonstrates, that the deletion introduced by CRISPR-Cas9 results in a functional *Prm1* null allele. PRM1 was detected in elongating spermatids and spermatozoa in wildtype (*Prm1*+/+) and *Prm1*+/- testis sections. PRM2 was present in all genotypes.

Mating of *Prm1*+/- males with *Prm1*+/- females produced approximately 50% *Prm1*+/- and 25% *Prm1*+/+ or *Prm1*-/- animals respectively (**Fig. 1d**), suggesting that the deletion did not interfere with embryonic development.

Prm1-/- *male mice are infertile, while Prm1*+/- *are subfertile*

After establishing and validating the *Prm1*-deficient line, we performed fertility tests with *Prm1*+/- and *Prm1*-/- males. *Prm1*+/- males are subfertile, while *Prm1*-/- males are sterile (**Fig. 1e**). None of the nine *Prm1*-/- males tested was able to generate offspring. *Prm1*+/- males generate smaller average litter sizes (mean: 3.81 ± 2.75) compared to WT males (mean: 6.75 ± 2.39) (**Fig. 1e**). Additionally, the pregnancy frequency of *Prm1*+/- males is significantly reduced (**Fig. 1f**). Only about 33% of the monitored copulations with *Prm1*+/- males resulted in pregnancies. These results indicate that loss of one allele of *Prm1* already reduces male mice fecundity.

Spermatogenesis unaffected in Prm1-deficient mice

In order to test, whether the deletion of *Prm1* affects spermatogenesis, we analyzed standard male fertility parameters. The relative testis mass (**Fig. 2a**), the average seminiferous tubuli diameter (**Fig. 2b**) and the number of elongating spermatids per seminiferous tubule cross section (**Fig. 2c**) are not reduced in *Prm1*+/- or *Prm1*-/- animals when compared with *Prm1*+/+ animals. Spermatozoa lining up at the lumen of stage VII-VIII seminiferous tubules can be detected in *Prm1*-deficient mice (**Fig. 2d**). Spermatids undergo differentiation, elongate and acrosomal structures and flagellae are formed in *Prm1*-deficient mice (**Fig. 2e**). These results suggest that spermatogenesis is unaffected in *Prm1*+/- and *Prm1*-/- mice.

Epididymal Prm1-deficient sperm display ROS-mediated DNA damage

Since PRM1 is necessary for DNA hypercondensation, we evaluated chromatin compaction of epididymal sperm. Transmission electron micrographs of epididymal sperm revealed defects in chromatin hypercondensation in *Prm1*-/- sperm compared to *Prm1*+/- and *Prm1*+/+

sperm (**Fig. 3a**). While approximately 80 - 85% of *Prm1+/-* and *Prm1+/+* epididymal sperm nuclei appear electron dense indicative for condensed chromatin, only around 29% of *Prm1-/-* sperm nuclei seem fully condensed (**Fig. 3b**). Additionally, epididymal sperm from *Prm1-/- mice* present with membrane damage and disrupted acrosomes in transmission electron micrographs (**Fig. 3c**).

To assess DNA damage, genomic DNA isolated from epididymal sperm was separated by agarose gel electrophoresis. DNA from WT sperm presents as a single band of high molecular weight indicative for intact DNA. Contrary, the majority of DNA isolated from *Prm1-/-* epididymal sperm is detected as fragments of approximately 100-500 bp indicative of strong DNA degradation. While DNA of sperm from *Prm2-/-* male mice is completely fragmented, a small proportion of DNA in *Prm1-/-* sperm is presented as a high molecular weight band indicating that a small portion of DNA from *Prm1-/-* sperm remains intact. DNA from *Prm1+/-* sperm displays a weak smear indicative for low, but detectable level of DNA-degradation (**Fig. 3d**). This suggests that loss of one *Prm1* allele leads to low levels of DNA damage. This is in contrast to *Prm2*, where loss of one allele was tolerated and DNA did not show any sign of degradation.

Since similar DNA damage have been described for *Prm2-/-* sperm and have been correlated to increased reactive oxygen species (ROS) levels during epididymal transit [32, 33], we stained testicular and epididymal tissue sections for 8-OHdG (8-hydroxydeoxyguanosine), a marker for oxidative stress induced DNA lesions. In tissue sections from epididymides of *Prm1-/-* mice, 60% of caput sperm and 64% of cauda sperm stained 8-OHdG-positive (**Fig. 3e-f**). In epididymides of *Prm1+/-* mice a small number of sperm stained positive for 8-OHdG (mean: 2.6% in caput and 3.0% in cauda epididymis). In contrast, on sections of *Prm1+/+* mice, no staining was detected. This shows, that the low level of DNA damage detected in *Prm1+/-* males is most likely restricted to the few 8-OHdG positive sperm and not due to low level of DNA damage in all sperm. Of note, the majority of the sperm from *Prm1-/-* mice stain 8-OHdG-positive in the testis (**Fig. 3f**).

389 *Epididymal Prm1-deficient sperm display impaired membrane integrity, nuclear head*
390 *morphology changes and sperm motility defects*

391 To characterize possible secondary effects of ROS, we next used Eosin-Nigrosin staining
392 and a hypoosmotic swelling test to test for sperm membrane integrity. *Prm1-/-* epididymal
393 sperm display severe membrane damage indicative of inviable sperm, while no significant
394 difference between *Prm1+/-* and *Prm1+/+* sperm was detected (**Fig. 4a, b, Supplementary**
395 **Fig. 2a, b**).

396 For analysis of epididymal sperm head morphology we used a high-throughput ImageJ
397 plugin [45] and generated a consensus shape visualizing the overall head shape of the
398 population analyzed. *Prm1-/-* sperm lose the typical hooked sperm head shape (**Fig. 4c,**
399 **Supplementary Fig. 3a**)**.** While the head shape of *Prm1-/-* sperm displays higher variability
400 (**Supplementary Fig. 3b**), they appear smaller with a mean area of 14.92 µm^2 (95% CI
401 14.92 ± 0.26) compared to 19.82 µm^2 (95% CI 19.82 ± 0.10) and 19.47 µm^2 (95% CI 19.47 ±
402 0.13) for *Prm1+/+* and *Prm1+/-* sperm heads, respectively (**Supplementary Fig. 3c**).
403 Further, *Prm1-/-* sperm heads are more elliptic (**Supplementary Fig. 3d**) and thinner
404 (**Supplementary Fig. 3e**). *Prm1+/-* sperm heads show a slightly stronger hook curvature
405 resulting in a reduced maximum ferret of 8.07 µm (95%b CI 8.07 ± 0.04) compared to 8.38
406 µm (95% CI 8.38 ± 0.04) for *Prm1+/+* sperm (**Supplementary Fig. 3f**). The reduction in
407 maximum ferret is significant, however, should be interpreted carefully, when considering the
408 general variability but clear overlap in sperm head shapes depicted for *Prm1+/-* and *Prm1+/+*
409 sperm populations (**Supplementary Fig. 3b**). These results suggest, that loss of one allele
410 of *Prm1* does not affect sperm head shape dramatically.

411 Next, we analyzed the percentage of motile sperm isolated from the cauda epididymis (**Fig.**
412 **4d**). Strikingly, *Prm1+/-* sperm showed a marked reduction in sperm motility. Only around
413 23% of the *Prm1+/-* sperm were motile. In contrast, 77% of WT sperm were motile, while
414 *Prm1*-deficient sperm are completely immotile. So, the reduction in motility contributes to the
415 sub/infertility seen.

416

Transcriptional and proteomic profiling reveals differences in Prm1 and Prm2 deficient males

To address the question, whether transcriptional silencing is affected upon loss of protamines, we performed transcriptomic and proteomic analyses. 3´-mRNA sequencing of the whole testis revealed that in *Prm1-/-* testis 99 genes are higher and 11 lower expressed, while in *Prm1+/-* testis 28 genes were higher and 39 were lower expressed, both compared to WT testis (**Fig. 5a, Supplementary Material 1**). In *Prm1-/-* testis pathway enrichment for immune related genes (*Il1b, Ccl5, Saa3, Atp6ap1, Rsad2, Cxcl10, Ifit1, Mmp13, Clec4e, Zghhc*) was identified. These transcripts were slightly higher abundant in *Prm1-/-* testis compared to WT testis, but showed low levels of expression (**Supplementary Material 1**). This might either indicate a reaction to ROS-mediated damage of the sperm in testis or an unspecific failure in transcriptional silencing.

In order to determine whether proteins might be differentially abundant in mature sperm, we analyzed basic nuclear protein extracts of *Prm1+/-*, *Prm1-/-*, *Prm2-/-* and WT sperm with MassSpec. In *Prm1-/-* samples 31 proteins were differentially abundant compared to WT sperm (**Fig. 5b, Supplementary Material 2**). Of these, 21 were also differentially abundant in *Prm2-/-* samples. Proteins related to translation, mRNA splicing and protein folding (EEF1A1, EEF1A2, RPL13, RPL31, SRSF1 and PPIA) were detected to be higher abundant in *Prm1-/-* or *Prm2-/-* sperm compared to WT sperm. Additionally, histones (H3F3, H3C) were found to be higher abundant in *Prm1-/-* and *Prm2-/-* sperm, indicating increased H3 histone retention. In addition, in *Prm2-/-* males also histone H4C was higher abundant. In *Prm1-/-* samples, further proteins were detected to be higher abundant related to translation and mRNA splicing (RPL8, RPS8, RPL18, RPL24, RPL26, SRSF3, SRSF7). Proteins related to stress response and apoptosis (B2M, CLU, HSPA2) were also higher abundant in sperm lacking PRM1 or PRM2. This we expected to be a stress response due to the increased ROS-mediated sperm damage detected. SMCP and SPESP1, proteins important for sperm motility and sperm-egg fusion on the other hand are lower abundant in both *Prm1-/-* and *Prm2-/-* samples. Only one protein, the ribosomal protein RPL31, which was also identified in *Prm1-/-* and *Prm2-/-* samples, was higher abundant in *Prm1+/-* sperm nuclear extracts

compared to WT sperm. The fact that there is only one non-protamine protein differentially abundant in *Prm1*+/- nuclear extracts, suggests that the *Prm1*+/- sperm protein profile is not causative of the subfertility observed.

Protamine and nuclear protein content are altered in protamine deficient epididymal sperm

Next, we analyzed the level of protamination using Chromomycin A3 (CMA3), a dye competing with protamines to bind CG-rich regions to the minor groove of DNA [47]. While 98% of *Prm1*+/- sperm show CMA3 staining, only around 29% of *Prm2*+/- sperm showed a CMA3-signal (**Fig. 6a, b**). These data suggest that chromatin in *Prm1*+/- and *Prm2*+/- sperm is either not fully or not correctly protaminated, with the effects being more dramatic in *Prm1*+/- sperm. Of note, sperm from *Prm1-/-* and *Prm2-/-* mice could not be analyzed due to the fact that severe DNA fragmentation interfered with the staining procedure.

To further analyze the relative protamine content and protamination of epididymal sperm of *Prm1*+/-, *Prm1-/-*, *Prm2*+/-, Prm2-/- and WT mice in more detail, basic nuclear proteins were separated on acid-urea polyacrylamide gels (AU-PAGE). Most interestingly, in sperm from *Prm1*+/- and *Prm1-/-* mice PRM2 precursors (pre-PRM2) were detected suggesting disturbances in processing of PRM2 upon loss of PRM1 (**Fig. 6c,** vermillion box). Further, we quantified the relative amounts of nuclear proteins within individual samples (**Fig. 6d-g, Supplementary Fig. 3**).

In WT epididymal sperm protamines account for around 86% of the total nuclear proteins (**Fig. 6d**). Interestingly, while the difference in sperm protamine content in *Prm1*+/- is not significant (83%), the protamine content is significantly reduced in sperm from *Prm2*+/- (78%), *Prm1-/-* (67%) and *Prm2-/-* (67%) mice (**Fig. 6d**). These results might help explaining the increased histone retention in *Prm1-/-* and *Prm2-/-* sperm, as detected by MassSpec.

While the relative amount of mPRM2 to total protamine is not significantly different in *Prm1*+/- and *Prm2*+/- sperm compared to WT (**Fig. 6e**), the total amount of PRM2 (mPRM2 + pre-PRM2) is significantly higher in *Prm1*+/- sperm (83%) only (**Fig. 6f**). Taking these data in account, in *Prm1*+/- sperm the PRM1:PRM2 ratio is shifted to approximately 1:5 while the

473 species-specific protamine ratio of 1:2 is maintained in *Prm2*+/- sperm which is comparable
474 to WT [14]. Consequently, the pre-PRM2 content of total PRM2 is significantly larger in
475 *Prm1*+/- and *Prm1*-/- sperm compared to *Prm2*+/- sperm (**Fig. 6g**).
476
477
478 **Discussion**
479
480 In this study, mice deficient for *Prm1* were generated using CRISPR-Cas9-mediated gene
481 editing. *Prm1*-/- male mice are infertile, while loss of one allele of *Prm1* results in subfertility.
482 *Prm1*-/- sperm show severe DNA fragmentation, high levels of 8-OHdG, destructed
483 membranes and complete immotility. *Prm1*+/- sperm show moderate ROS-induced DNA
484 damage, reduced sperm motility and a shifted PRM1:PRM2 ratio. *Prm1*-/- and *Prm1*+/-
485 sperm contain high levels of incompletely processed PRM2 suggesting that PRM1 is
486 necessary for correct PRM2 processing.
487 Protamine deficient mouse models have been described and associated with male factor
488 infertility in previous studies [28-31]. Contrary to previous studies, we show that *Prm1*+/-
489 males are able to produce offspring by natural breeding. *Prm1*-deficient chimeras, that have
490 been generated by classical gene-targeting techniques, were reported to be sterile [28],
491 excluding mouse line establishment and detailed studies on *Prm1*-deficiency. Takeda *et al.*
492 were, however, able to generate viable offspring from *Prm1*+/- males by *in vitro* fertilization
493 (IVF) of zona-free oocytes [30]. Further, Mashiko *et al.* reported that CRISPR-Cas9-mediated
494 *Prm1*+/- mice are infertile, however detailed fertility statistics and phenotypical analysis of
495 *Prm1*-deficient mice were not performed [31]. Since the *Prm1*+/- males produced by us are
496 subfertile, we were able to generate and analyze *Prm1*-/- mice. Takeda *et al.* used a different
497 mouse strain (C57BL/6J x DBA, backcrossed to CD1) and ES-targeting technology, which
498 might explain the differences in *Prm1*+/- fertility. While Mashiko *et al.* used both the identical
499 strain (C57BL/6J x DBA, backcrossed to C57BL/6J) and technology, they might not have
500 performed a sufficiently exhaustive fertility analysis in order to detect subfertility.

Spermatogenesis seems unaffected in *Prm1*-/- (and *Prm1*+/-) mice compared to WT mice. Similar results were described for *Prm2*-/- mice, where spermatogenesis appears normal [32], epididymal sperm however show severe damage. In *Prm2*-/- mice it has been reported that an oxidative stress-mediated destruction cascade is initiated during epididymal sperm maturation [32, 33]. While it is well known that low levels of ROS are required for proper sperm function, high levels cause sperm pathologies [48]. Accumulation of ROS and loss of the antioxidant capacity of *Prm2*-/- sperm caused severe DNA fragmentation, sperm immotility and sperm membrane damage. We observe even earlier effects in *Prm1*-/- mice displaying ROS-mediated DNA damage already in the testis subsequently leading to immotility and disrupted membranes. Thus, loss of *Prm1* renders the ROS system more fragile at an even earlier stage. Additionally, transcriptional silencing seems impaired in *Prm1-/-* and *Prm2-/-* [33] sperm as indicated by differential gene expression analysis in testis. Further, we detected increased histone retention in *Prm1-/-* and *Prm2-/-* sperm using MassSpec. Differential abundance analysis of nuclear proteins in *Prm1-/-* and *Prm2-/-* epididymal sperm show proteins related to translation and apoptotic processes consistent with the secondary effects observed. However, only moderate differences were detected in *Prm1*+/- sperm compared to WT indicating that these changes most likely do not contribute to the phenotype observed.

While *Prm1-/-* male mice display a phenocopy of *Prm2-/-* male mice, marked differences were found between heterozygous males. Interestingly, *Prm1*+/- males are subfertile showing a reduction in average litter sizes and lower pregnancy frequencies. Of note, *Prm2*+/- are fertile [32]. This suggests that loss of one allele of *Prm1*, in contrast to loss of one allele of *Prm2*, cannot be tolerated. Transmission electron micrographs revealed that DNA of *Prm1*+/- sperm appears electron dense suggesting that the chromatin in sperm is condensed to the same level as *Prm2*+/- [32] and WT sperm. This raises the question as to why *Prm1*+/- males are subfertile.

We show that a small population of *Prm1*+/- epididymal sperm stain 8-OHdG positive. Also, genomic DNA isolated from *Prm1*+/- sperm is partially fragmented. This indicates that some

sperm experience DNA damage caused by ROS rather than all sperm bearing some degree of DNA damage. Surprisingly, however, we did not detect marked differences in chromatin condensation or membrane integrity between WT and *Prm1*+/- sperm. *Prm2*+/- sperm did not show an increase in ROS-mediated DNA damage compared to WT sperm [33]. Thus, *Prm1*+/- sperm seem more sensible or more exposed to oxidative stress mediated damage compared to *Prm2*+/- sperm. This might contribute to the subfertility of *Prm1*+/- males.

Noteworthy, redox imbalance in sperm has been repeatedly connected not only to sperm DNA damage, but also reduced sperm motility in men [49]. It has been reported that sperm mitochondria present a significant source of ROS in defective sperm [50]. In human, spontaneous production of mitochondrial ROS by defective sperm causes peroxidative damage to the sperm midpiece leading to reduced sperm motility. One of the major differences between *Prm1*+/- and *Prm2*+/- sperm is that loss of one allele of *Prm1* leads to a marked decrease in sperm motility, whereas *Prm2*+/- sperm motility was not significantly different from WT sperm [32]. Only around 23% of the *Prm1*+/- sperm are motile, an amount that qualifies in human as asthenozoospermic according to the WHO criteria [49, 51, 52]. Since mitochondrial ROS has been negatively correlated to sperm motility and we detect a moderate increase in ROS in *Prm1*+/- sperm compared to WT, we believe that reduced sperm motility in *Prm1*+/- males is (at least partially) caused by ROS, which contributes to the subfertility observed in *Prm1*+/- males.

Another notable difference between *Prm1*+/- and *Prm2*+/- sperm is the aberrant DNA protamination as revealed by CMA3 staining. While approximately one third of the *Prm2*+/- sperm stain with CMA3, around 98% of *Prm1*+/- sperm are CMA3-positive. For human ejaculates, the percentage of CMA3-positive sperm varies considerably [53] and values of up to 30% CMA3-positive sperm have been defined for normal semen samples of fertile men [54, 55]. Thus, we argue that the 29% CMA3-positive sperm seen in *Prm2*+/- males, despite being higher than the values detected in WT controls, can be tolerated and do not affect regular fertility. However, it is surprising that only 2% of CMA3-negative sperm in *Prm1*+/- mice still result in a partially retained fertility. Enhanced CMA3-staining of sperm is correlated

with increased histone retention. Surprisingly, the high CMA3 level in *Prm1+/-* sperm could not be correlated with increased histone retention as shown by MassSpec. One possible explanation for the intense CMA3 staining in *Prm1+/-* sperm could be the vast amounts of pre-PRM2 detected in nuclear protein extracts from epididymal sperm. We hypothesize that failure of processing of pre-PRM2 and pre-PRM2 loading onto sperm DNA might allow the intercalating dye to access DNA and stain the chromatin.

Defects in PRM2 processing were also described for histone variant H2A.L.2-KO, transition protein (TPs)-1 and -2 (TP1/TP2)-double KO, TP2-KO and cleaved PRM2 cP2-KO mouse models [40, 56-58], all of which display fertility problems. Interestingly, a recent study showed that mutation of a single non-arginine residue in PRM1 ($P1^{K49A/K49A}$) leads to impaired PRM2 processing in mice [59]. Of note, *Prm2+/-* sperm contain scarce amounts of pre-PRM2 as well. The relative amount of pre-PRM2 is, however, significantly larger *in Prm1+/-* sperm. Hence, species-specific PRM1 levels are required for proper PRM2 processing and alterations of these levels unequivocally lead to reduced fertility. Noteworthy, presence of pre-PRM2 in subfertile human sperm has been described before [19].

In addition to high levels of pre-PRM2, *Prm1+/-* sperm display a shift in the PRM1:PRM2 ratio from approximately 1:2 in WT sperm to 1:5 in *Prm1+/-* sperm. Also, in cP2-deficient mice a shift in the protamine ratio has been described. Arévalo *et al.* have shown that mice lacking the highly conserved N-terminal part of PRM2, called cleaved PRM2 (cP2), display defective PRM2 processing and show a PRM1:PRM2 ratio of approx. 5:1 [40]. Mice lacking cP2 on one allele are infertile. As *Prm1+/-* males are subfertile, it appears that a ratio of 1:5 can be tolerated to some extent, whereas a 5:1 ratio is incompatible with fertility. Of note, the protamine ratio in *Prm2+/-* sperm is not significantly different from WT sperm explaining their regular fertility. In human, alterations of the species-specific ratio both on protein and transcript level have been repeatedly correlated to male sub- and infertility[15-27]. These results once again underline the importance of the protamine ratio in species expressing both protamines.

584 Of note, the protamine ratio in mice harboring a C-terminally altered allele of protamine 1
585 ($P1^{K49A/K49A}$) was, contrary to the *Prm1*+/- sperm analyzed here, unaltered [59]. $P1^{K49A/K49A}$
586 mice are, like *Prm1*+/- mice subfertile. Interestingly, $P1^{K49A/K49A}$ sperm show increased
587 histone retention similar to *Prm1-/-* and *Prm2-/-* sperm which is not detected in *Prm1* +/-
588 sperm. Thus, the presence of one functional *Prm1* allele is sufficient for proper histone
589 eviction.
590
591 In summary, we generated and characterized *Prm1*-deficient mice. We demonstrate that
592 *Prm1*+/- mice are subfertile, exhibiting sperm with moderate ROS-induced DNA damage and
593 reduced motility. Opposed to *Prm2*+/- sperm, large amounts of pre-PRM2 were detected in
594 *Prm1*+/- sperm. While the crucial species-specific protamine ratio is maintained in *Prm2*+/-
595 sperm, *Prm1*+/- sperm exhibit an aberrant protamine ratio. We demonstrate that *Prm1-/-* and
596 *Prm2-/-* mice display impaired transcriptional silencing, increased histone retention and redox
597 imbalance leading to severe sperm damage, which render males infertile. Loss of *Prm1*
598 seemingly triggers the ROS system at an even earlier stage compared to loss of *Prm2*. By
599 intercrossing the *Prm1*-deficient mouse line presented here to our published *Prm2*+/- model,
600 we will next generate and analyze *Prm1*+/- *Prm2*+/- double heterozygous males, which will
601 further advance our knowledge about the molecular consequences of disturbances in PRM1
602 and PRM2 levels and the PRM1:PRM2 ratio.
603
604
605 **Acknowledgements**
606 This study was supported by grants from the Deutsche Forschungsgemeinschaft (DFG) to
607 HS (SCHO 503/23-1), LA (AR 1221/1-1) and KS (STE 892/19-1). We thank Gaby Beine,
608 Andrea Jäger, Angela Egert, Irina Kosterin, Anna Pehlke, Greta Zech, Barbara Fröhlich and
609 Tania Bloch for excellent technical assistance. Protein identifications were done at the
610 University of Bonn Core Facility Mass Spectrometry, Institute of Biochemistry and Molecular
611 Biology, Medical Faculty, University of Bonn funded by the Deutsche

612 Forschungsgemeinschaft (DFG) – Projektnummer 386936527. We would like to
613 acknowledge the assistance of the University Bonn Core Facility Next Generation
614 Sequencing (NGS) for their support.

615

616

617 **Author contributions**

618 G.E.M., K.S., and H.S. conceptualized the study. S.S. generated gene-edited mice. G.E.M.,
619 J.M., L.A., S.S., A.F. and A.K. analyzed mice. G.E.M. and H.S. drafted the manuscript. All
620 authors read and approved the final manuscript.

621

622

623 **References**

624 1. Rathke C, Baarends WM, Awe S, Renkawitz-Pohl R. Chromatin dynamics during
625 spermiogenesis. Biochim Biophys Acta. 2014;1839(3):155-68. doi:
626 10.1016/j.bbagrm.2013.08.004.
627 2. Balhorn R. A model for the structure of chromatin in mammalian sperm. J Cell Biol.
628 1982;93(2):298-305. doi: 10.1083/jcb.93.2.298.
629 3. Steger K. Transcriptional and translational regulation of gene expression in haploid
630 spermatids. Anat Embryol (Berl). 1999;199(6):471-87. doi: 10.1007/s004290050245.
631 4. Chauviere M, Martinage A, Debarle M, Sautiere P, Chevaillier P. Molecular
632 characterization of six intermediate proteins in the processing of mouse protamine P2
633 precursor. Eur J Biochem. 1992;204(2):759-65. doi: 10.1111/j.1432-1033.1992.tb16691.x.
634 5. Retief JD, Dixon GH. Evolution of pro-protamine P2 genes in primates. Eur J Biochem.
635 1993;214(2):609-15. doi: 10.1111/j.1432-1033.1993.tb17960.x.

636 6. Reeves RH, Gearhart JD, Hecht NB, Yelick P, Johnson P, O'Brien SJ. Mapping of PRM1
637 to human chromosome 16 and tight linkage of Prm-1 and Prm-2 on mouse chromosome 16.
638 J Hered. 1989;80(6):442-6. doi: 10.1093/oxfordjournals.jhered.a110895.
639 7. Wykes SM, Krawetz SA. Conservation of the PRM1 --> PRM2 --> TNP2 domain. DNA
640 Seq. 2003;14(5):359-67. doi: 10.1080/10425170310001599453.
641 8. Balhorn R. The protamine family of sperm nuclear proteins. Genome Biol.
642 2007;8(9):227. doi: 10.1186/gb-2007-8-9-227.
643 9. Yelick PC, Balhorn R, Johnson PA, Corzett M, Mazrimas JA, Kleene KC, et al. Mouse
644 protamine 2 is synthesized as a precursor whereas mouse protamine 1 is not. Mol Cell Biol.
645 1987;7(6):2173-9. doi: 10.1128/mcb.7.6.2173.
646 10. Krawetz SA, Dixon GH. Sequence similarities of the protamine genes: implications for
647 regulation and evolution. J Mol Evol. 1988;27(4):291-7. doi: 10.1007/BF02101190.
648 11. Luke L, Tourmente M, Roldan ER. Sexual Selection of Protamine 1 in Mammals. Mol
649 Biol Evol. 2016;33(1):174-84. doi: 10.1093/molbev/msv209.
650 12. Luke L, Tourmente M, Dopazo H, Serra F, Roldan ER. Selective constraints on
651 protamine 2 in primates and rodents. BMC Evol Biol. 2016;16:21. doi: 10.1186/s12862-016-
652 0588-1.
653 13. de Mateo S, Gazquez C, Guimera M, Balasch J, Meistrich ML, Ballesca JL, et al.
654 Protamine 2 precursors (Pre-P2), protamine 1 to protamine 2 ratio (P1/P2), and assisted
655 reproduction outcome. Fertil Steril. 2009;91(3):715-22. doi:
656 10.1016/j.fertnstert.2007.12.047.
657 14. Corzett M, Mazrimas J, Balhorn R. Protamine 1: protamine 2 stoichiometry in the
658 sperm of eutherian mammals. Mol Reprod Dev. 2002;61(4):519-27. doi: 10.1002/mrd.10105.

15. Aoki VW, Moskovtsev SI, Willis J, Liu L, Mullen JB, Carrell DT. DNA integrity is compromised in protamine-deficient human sperm. J Androl. 2005;26(6):741-8. doi: 10.2164/jandrol.05063.

16. Balhorn R, Reed S, Tanphaichitr N. Aberrant protamine 1/protamine 2 ratios in sperm of infertile human males. Experientia. 1988;44(1):52-5. doi: 10.1007/BF01960243.

17. Belokopytova IA, Kostyleva EI, Tomilin AN, Vorob'ev VI. Human male infertility may be due to a decrease of the protamine P2 content in sperm chromatin. Mol Reprod Dev. 1993;34(1):53-7. doi: 10.1002/mrd.1080340109.

18. Bench G, Corzett MH, de Yebra L, Oliva R, Balhorn R. Protein and DNA contents in sperm from an infertile human male possessing protamine defects that vary over time. Mol Reprod Dev. 1998;50(3):345-53. doi: 10.1002/(SICI)1098-2795(199807)50:3<345::AID-MRD11>3.0.CO;2-3.

19. de Yebra L, Ballesca JL, Vanrell JA, Corzett M, Balhorn R, Oliva R. Detection of P2 precursors in the sperm cells of infertile patients who have reduced protamine P2 levels. Fertil Steril. 1998;69(4):755-9. doi: 10.1016/s0015-0282(98)00012-0.

20. Garcia-Peiro A, Martinez-Heredia J, Oliver-Bonet M, Abad C, Amengual MJ, Navarro J, et al. Protamine 1 to protamine 2 ratio correlates with dynamic aspects of DNA fragmentation in human sperm. Fertil Steril. 2011;95(1):105-9. doi: 10.1016/j.fertnstert.2010.06.053.

21. Khara KK, Vlad M, Griffiths M, Kennedy CR. Human protamines and male infertility. J Assist Reprod Genet. 1997;14(5):282-90. doi: 10.1007/BF02765830.

22. Ni K, Spiess AN, Schuppe HC, Steger K. The impact of sperm protamine deficiency and sperm DNA damage on human male fertility: a systematic review and meta-analysis. Andrology. 2016;4(5):789-99. doi: 10.1111/andr.12216.

683 23. Oliva R. Protamines and male infertility. Hum Reprod Update. 2006;12(4):417-35. doi:
684 10.1093/humupd/dml009.
685 24. Steger K, Failing K, Klonisch T, Behre HM, Manning M, Weidner W, et al. Round
686 spermatids from infertile men exhibit decreased protamine-1 and -2 mRNA. Hum Reprod.
687 2001;16(4):709-16. doi: 10.1093/humrep/16.4.709.
688 25. Steger K, Fink L, Failing K, Bohle RM, Kliesch S, Weidner W, et al. Decreased
689 protamine-1 transcript levels in testes from infertile men. Mol Hum Reprod. 2003;9(6):331-
690 6. doi: 10.1093/molehr/gag041.
691 26. Steger K, Wilhelm J, Konrad L, Stalf T, Greb R, Diemer T, et al. Both protamine-1 to
692 protamine-2 mRNA ratio and Bcl2 mRNA content in testicular spermatids and ejaculated
693 spermatozoa discriminate between fertile and infertile men. Hum Reprod. 2008;23(1):11-6.
694 doi: 10.1093/humrep/dem363.
695 27. Torregrosa N, Dominguez-Fandos D, Camejo MI, Shirley CR, Meistrich ML, Ballesca JL,
696 et al. Protamine 2 precursors, protamine 1/protamine 2 ratio, DNA integrity and other sperm
697 parameters in infertile patients. Hum Reprod. 2006;21(8):2084-9. doi:
698 10.1093/humrep/del114.
699 28. Cho C, Willis WD, Goulding EH, Jung-Ha H, Choi YC, Hecht NB, et al.
700 Haploinsufficiency of protamine-1 or -2 causes infertility in mice. Nat Genet. 2001;28(1):82-
701 6. doi: 10.1038/ng0501-82.
702 29. Cho C, Jung-Ha H, Willis WD, Goulding EH, Stein P, Xu Z, et al. Protamine 2 deficiency
703 leads to sperm DNA damage and embryo death in mice. Biol Reprod. 2003;69(1):211-7. doi:
704 10.1095/biolreprod.102.015115.

705 30. Takeda N, Yoshinaga K, Furushima K, Takamune K, Li Z, Abe S, et al. Viable offspring
706 obtained from Prm1-deficient sperm in mice. Sci Rep. 2016;6:27409. doi:
707 10.1038/srep27409.
708 31. Mashiko D, Fujihara Y, Satouh Y, Miyata H, Isotani A, Ikawa M. Generation of mutant
709 mice by pronuclear injection of circular plasmid expressing Cas9 and single guided RNA. Sci
710 Rep. 2013;3:3355. doi: 10.1038/srep03355.
711 32. Schneider S, Balbach M, Jan FJ, Fietz D, Nettersheim D, Jostes S, et al. Re-visiting the
712 Protamine-2 locus: deletion, but not haploinsufficiency, renders male mice infertile. Sci Rep.
713 2016;6:36764. doi: 10.1038/srep36764.
714 33. Schneider S, Shakeri F, Trotschel C, Arevalo L, Kruse A, Buness A, et al. Protamine-2
715 Deficiency Initiates a Reactive Oxygen Species (ROS)-Mediated Destruction Cascade during
716 Epididymal Sperm Maturation in Mice. Cells. 2020;9(8). doi: 10.3390/cells9081789.
717 34. Weyrich A. Preparation of genomic DNA from mammalian sperm. Curr Protoc Mol
718 Biol. 2012;Chapter 2:Unit 2 13 1-3. doi: 10.1002/0471142727.mb0213s98.
719 35. Kim D, Langmead B, Salzberg SL. HISAT: a fast spliced aligner with low memory
720 requirements. Nat Methods. 2015;12(4):357-60. doi: 10.1038/nmeth.3317.
721 36. Pertea M, Pertea GM, Antonescu CM, Chang TC, Mendell JT, Salzberg SL. StringTie
722 enables improved reconstruction of a transcriptome from RNA-seq reads. Nat Biotechnol.
723 2015;33(3):290-5. doi: 10.1038/nbt.3122.
724 37. Robinson JT, Thorvaldsdottir H, Winckler W, Guttman M, Lander ES, Getz G, et al.
725 Integrative genomics viewer. Nat Biotechnol. 2011;29(1):24-6. doi: 10.1038/nbt.1754.
726 38. Love MI, Huber W, Anders S. Moderated estimation of fold change and dispersion for
727 RNA-seq data with DESeq2. Genome Biol. 2014;15(12):550. doi: 10.1186/s13059-014-0550-
728 8.

729 39. Mi H, Huang X, Muruganujan A, Tang H, Mills C, Kang D, et al. PANTHER version 11:
730 expanded annotation data from Gene Ontology and Reactome pathways, and data analysis
731 tool enhancements. Nucleic Acids Res. 2017;45(D1):D183-D9. doi: 10.1093/nar/gkw1138.
732 40. Arévalo L, Merges GE, Schneider S, Oben FE, Neumann I, Schorle H. Loss of the
733 cleaved-protamine 2 domain leads to incomplete histone-to-protamine exchange and
734 infertility in mice. Biorxiv. 2021. doi: 10.1101/2021.09.29.462440.
735 41. Mellacheruvu D, Wright Z, Couzens AL, Lambert JP, St-Denis NA, Li T, et al. The
736 CRAPome: a contaminant repository for affinity purification-mass spectrometry data. Nat
737 Methods. 2013;10(8):730-6. doi: 10.1038/nmeth.2557.
738 42. Kall L, Storey JD, MacCoss MJ, Noble WS. Assigning significance to peptides identified
739 by tandem mass spectrometry using decoy databases. J Proteome Res. 2008;7(1):29-34. doi:
740 10.1021/pr700600n.
741 43. Ahlmann-Eltze C, Anders S. proDA: Probabilistic dropout analysis for identifying
742 differentially abundant proteins in label-free mass spectrometry. Biorxiv. 2021.
743 44. Wickham H. ggplot2. Wiley Interdisciplinary Reviews: Computational Statistics. 2011.
744 45. Skinner BM, Rathje CC, Bacon J, Johnson EEP, Larson EL, Kopania EEK, et al. A high-
745 throughput method for unbiased quantitation and categorization of nuclear
746 morphologydagger. Biol Reprod. 2019;100(5):1250-60. doi: 10.1093/biolre/ioz013.
747 46. Soler-Ventura A, Castillo J, de la Iglesia A, Jodar M, Barrachina F, Ballesca JL, et al.
748 Mammalian Sperm Protamine Extraction and Analysis: A Step-By-Step Detailed Protocol and
749 Brief Review of Protamine Alterations. Protein Pept Lett. 2018;25(5):424-33. doi:
750 10.2174/0929866525666180412155205.
751 47. Sadeghi S, Talebi AR, Shahedi A, Moein MR, Abbasi-Sarcheshmeh A. Effects of
752 Tamoxifen on DNA Integrity in Mice. J Reprod Infertil. 2019;20(1):10-5.

753 48. de Lamirande E, Jiang H, Zini A, Kodama H, Gagnon C. Reactive oxygen species and
754 sperm physiology. Rev Reprod. 1997;2(1):48-54. doi: 10.1530/ror.0.0020048.
755 49. Alahmar AT. Role of Oxidative Stress in Male Infertility: An Updated Review. J Hum
756 Reprod Sci. 2019;12(1):4-18. doi: 10.4103/jhrs.JHRS_150_18.
757 50. Koppers AJ, De Iuliis GN, Finnie JM, McLaughlin EA, Aitken RJ. Significance of
758 mitochondrial reactive oxygen species in the generation of oxidative stress in spermatozoa. J
759 Clin Endocrinol Metab. 2008;93(8):3199-207. doi: 10.1210/jc.2007-2616.
760 51. Cooper TG, Noonan E, von Eckardstein S, Auger J, Baker HW, Behre HM, et al. World
761 Health Organization reference values for human semen characteristics. Hum Reprod Update.
762 2010;16(3):231-45. doi: 10.1093/humupd/dmp048.
763 52. WHO laboratory manual for the examination and processing of human semen [press
764 release]. Geneva: World Health Organization2010.
765 53. Lolis D, Georgiou I, Syrrou M, Zikopoulos K, Konstantelli M, Messinis I. Chromomycin
766 A3-staining as an indicator of protamine deficiency and fertilization. Int J Androl.
767 1996;19(1):23-7. doi: 10.1111/j.1365-2605.1996.tb00429.x.
768 54. Sakkas D, Urner F, Bianchi PG, Bizzaro D, Wagner I, Jaquenoud N, et al. Sperm
769 chromatin anomalies can influence decondensation after intracytoplasmic sperm injection.
770 Hum Reprod. 1996;11(4):837-43. doi: 10.1093/oxfordjournals.humrep.a019263.
771 55. Zandemami M, Qujeq D, Akhondi MM, Kamali K, Raygani M, Lakpour N, et al.
772 Correlation of CMA3 Staining with Sperm Quality and Protamine Deficiency. Lab Med.
773 2012;43. doi: 10.1309/LMB42F9QXYKFLJNG.
774 56. Zhao M, Shirley CR, Yu YE, Mohapatra B, Zhang Y, Unni E, et al. Targeted disruption of
775 the transition protein 2 gene affects sperm chromatin structure and reduces fertility in mice.
776 Mol Cell Biol. 2001;21(21):7243-55. doi: 10.1128/MCB.21.21.7243-7255.2001.

777 57. Barral S, Morozumi Y, Tanaka H, Montellier E, Govin J, de Dieuleveult M, et al.
778 Histone Variant H2A.L.2 Guides Transition Protein-Dependent Protamine Assembly in Male
779 Germ Cells. Mol Cell. 2017;66(1):89-101 e8. doi: 10.1016/j.molcel.2017.02.025.
780 58. Shirley CR, Hayashi S, Mounsey S, Yanagimachi R, Meistrich ML. Abnormalities and
781 reduced reproductive potential of sperm from Tnp1- and Tnp2-null double mutant mice. Biol
782 Reprod. 2004;71(4):1220-9. doi: 10.1095/biolreprod.104.029363.
783 59. Moritz L, Schon SB, Rabbani M, Sheng Y, Pendlebury DF, Agrawal R, et al. Single
784 residue substitution in protamine 1 disrupts sperm genome packaging and embryonic
785 development in mice. bioRxiv. 2021. doi: 10.1101/2021.09.16.460631.
786

Figure Legends

Fig.1. Establishment of *Prm1*-deficient mice and fertility analysis. (a) Graphical representation of CRISPR-Cas9-mediated gene editing of the *Prm1* locus. Two guide RNAs were used (indicated by black arrow heads); targeting the *Prm1* coding sequence in exon 1 and exon 2, respectively. A 167 bp in-frame deletion was generated, leading to loss of crucial arginine-rich DNA binding sites (marked in blue). The epitope of the anti-PRM1 antibody used in Fig.1c is marked in red. **(b)** Agarose gel of genotyping polymerase chain reaction of *Prm1*+/+, *Prm1*+/- and *Prm1*-/- mice. Amplification of the wild type *Prm1* or the *Prm1*- allele generates products of 437 bp or 270 bp, respectively. L = ladder **(c)** Immunohistochemical staining against PRM1 and PRM2 on Bouin-fixed, paraffin-embedded testis sections of *Prm1*+/+, *Prm1*+/- and *Prm1*-/- mice counterstained with hematoxylin. Scale: 50 µm **(d)** Mendelian distribution of genotypes (n = 10 litters) from crossings of *Prm1*+/- males and females. **(e)** Scatter plot of litter sizes monitored after mating with female WT C57BL/6J mice. n = number of pregnancies produced by 12 *Prm1*+/+, 9 *Prm1*+/- and 9 *Prm1*-/- males, respectively. The mean litter size is indicated by vermillion lines. **(f)** Pregnancy frequency (%) after mating with female WT C57BL/6J mice. n = number of plugs produced by 12 *Prm1*+/+, 9 *Prm1*+/- and 9 *Prm1*-/- males, respectively.

Fig.2. Spermatogenesis of *Prm1*-deficient mice. (a) Testis to body weight ratio of *Prm1*+/+, *Prm1*+/- and *Prm1*-/- males (n = 8-10). **(b)** Average diameter of seminiferous tubules of *Prm1*+/+, *Prm1*+/- and *Prm1*-/- mice (n = 4). 25 tubules per mouse were evaluated. **(c)** Quantification of elongating spermatids per seminiferous tubule cross-section in *Prm1*+/+, *Prm1*+/- and *Prm1*-/- males (n = 3). 5 tubules per mouse were evaluated. **(d)** Hematoxylin-Eosin staining of testis of *Prm1*+/+, *Prm1*+/- and *Prm1*-/- males. Tubules at stage VII-VIII of the epithelial cycle with spermatozoa lining up at the edge of tubule lumen are marked with asterisks. Scale: 50 µm **(e)** Periodic acid Schiff staining of testis of *Prm1*+/+,

Prm1+/- and *Prm1*-/- males. Acrosomal structures are indicated by vermillion arrow heads. Scale: 50 µm

Fig.3. Analysis of chromatin condensation and ROS-induced DNA damage in epididymal *Prm1*-deficient sperm. (a) Representative transmission electron micrographs of *Prm1*+/+, *Prm1*+/- and *Prm1*-/- epididymal sperm. Scale: 2 µm **(b)** Quantification of DNA condensation of epididymal sperm from *Prm1*+/+, *Prm1*+/- and *Prm1*-/- males (n = 3). 100 sperm per male were analyzed. **(c)** Transmission electron micrograph of *Prm1*-/- epididymal sperm. Scale: 2 µm **(d)** Agarose gel loaded with genomic DNA isolated from epididymal sperm of *Prm1*+/-, *Prm1*-/-, *Prm2*+/-, *Prm2*-/- and WT males separated by electrophoresis. L = ladder **(e)** Percentage of 8-OHdG positive sperm on tissue sections of caput and cauda epididymis of *Prm1*+/+, *Prm1*+/- and *Prm1*-/- mice (n =3). **(f)** Representative immunofluorescent staining against 8-OHdG in testis, caput epididymis and cauda epididymis tissue sections from *Prm1*+/+, *Prm1*+/- and *Prm1*-/- males. Scale: 50 µm

Fig.4. Secondary effects on *Prm1*-deficient epididymal sperm. (a) Eosin-Nigrosin (EN) staining: Quantification of EN positive and EN negative sperm (%) from *Prm1*+/+, *Prm1*+/- and *Prm1*-/- males. (n = 5) **(b)** Hyperosmotic swelling test: Quantification of HOS positive and HOS negative sperm (%) from *Prm1*+/+, *Prm1*+/- and *Prm1*-/- males (n =3). **(c)** Nuclear head morphology analysis for *Prm1*+/+, *Prm1*+/- and *Prm1*-/- sperm. Consensus shapes of sperm heads are depicted. 4 males per genotype and a minimum of 100 sperm per animal were analyzed. **(d)** Quantification of motile and immotile sperm (%) from *Prm1*+/+, *Prm1*+/- and *Prm1*-/- males (n = 3).

Fig.5. Differentially expressed genes in the testis and altered protein abundances in sperm in protamine-deficient males. (a) Number of differentially expressed genes subdivided into higher and lower expressed genes in testis of *Prm1*+/- and *Prm1*-/- males compared to WT males, respectively. **(b)** Venn diagram illustrating changes in abundances

of proteins from sperm nuclear protein extractions of *Prm1-/-*, *Prm1+/-* and *Prm2-/-* males compared to WT, respectively. Proteins that were higher abundant are depicted in bold letters. Non-bold proteins were lower abundant compared to WT.

Fig.6. Sperm nuclear protein analysis in protamine-deficient sperm. (a) Representative pictures of CMA3 staining of *Prm1+/+*, *Prm1+/-* and *Prm2+/-* epididymal sperm heads taken at same exposure time. DAPI was used as counter stain. Scale: 20 µm. **(b)** Average percentage of CMA3 positive and negative sperm in *Prm1+/-*, *Prm2+/-* and WT males (n = 3). A minimum of 400 sperm per male were analyzed. **(c)** Representative acid-urea polyacrylamide gel (AU-PAGE) of nuclear protein extractions from WT, *Prm1+/-*, *Prm1-/-, Prm2+/-* and *Prm2-/-* epididymal sperm. Non-protamine nuclear proteins can be detected at the top of the AU-PAGE. PRM1 and PRM2 run at the bottom of the gel. PRM2 precursor forms (pre-PRM2) run higher than PRM (marked by vermillion box). **(d)** Percentage of PRM of total nuclear protein in nuclear protein extractions from WT, *Prm1+/-*, *Prm1-/-, Prm2+/-* and *Prm2-/-* epididymal sperm. **(e)** Percentage of mPRM2 of PRM in nuclear protein extractions from WT, *Prm1+/-* and *Prm2+/-* epididymal sperm. **(f)** Percentage of total PRM2 (including pre-PRM2) of PRM in nuclear protein extractions from WT, *Prm1+/-* and *Prm2+/-* epididymal sperm. **(g)** Percentage of pre-PRM2 of PRM2 in nuclear protein extractions from *Prm1+/-, Prm1-/-* and *Prm2+/-* epididymal sperm.

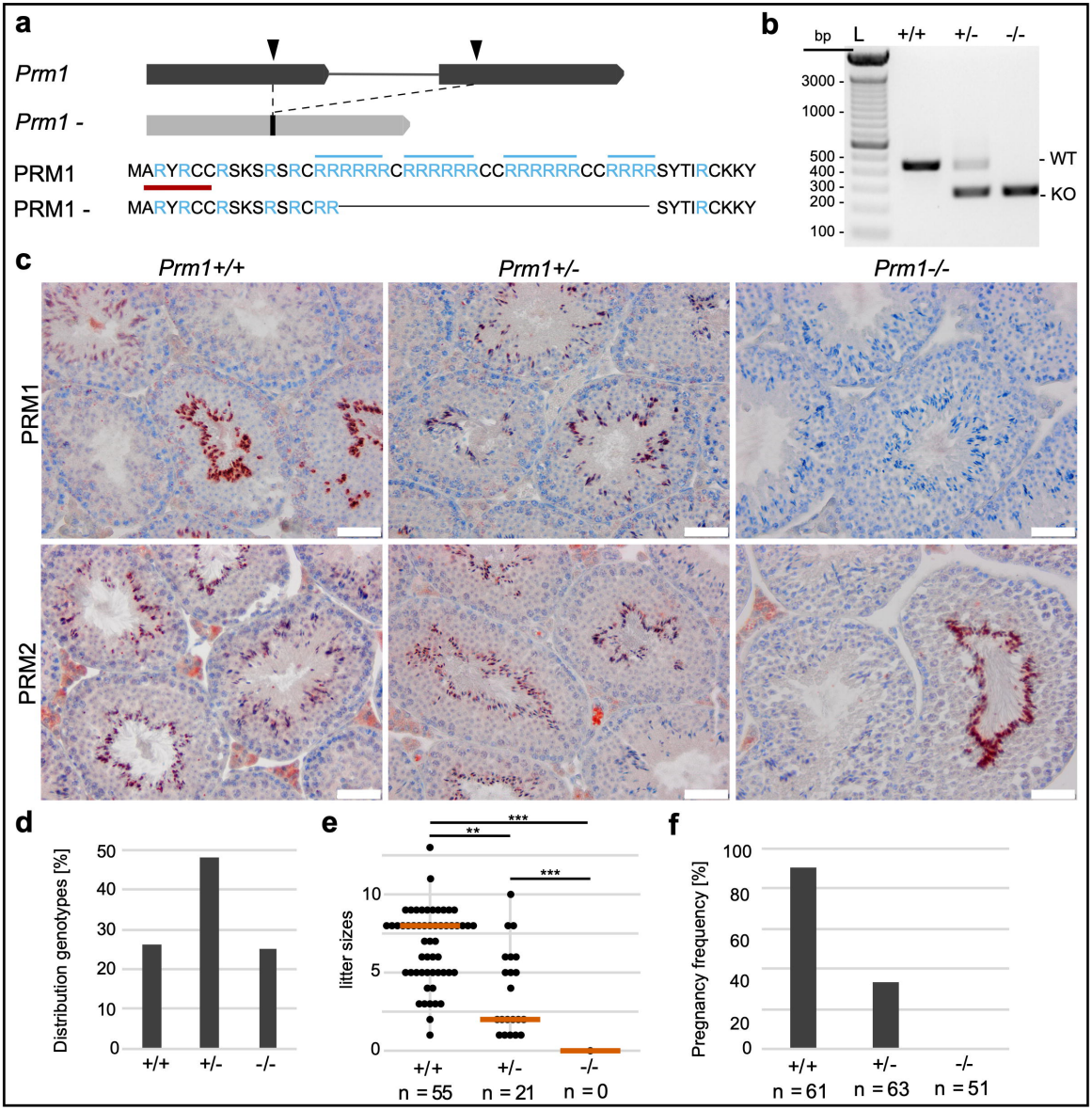
a
Prm1
Prm1 -
PRM1
MARYRCCRSKSRSRCRRRRRRCRRRRRRCCRRRRRRCCRRRRSYTIRCKKY
PRM1 -
MARYRCCRSKSRSRCRR
SYTIRCKKY
b
bp
L
+/+
+/-
-/-
3000
1000
500
400
300
200
100
WT
KO
c
Prm1+/+
Prm1+/-
Prm1-/-
PRM1
PRM2
d
Distribution genotypes [%]
50
40
30
20
10
0
+/+
+/-
-/-
e
litter sizes
10
5
0
***
**
***
+/+
+/-
-/-
n = 55
n = 21
n = 0
f
Pregnancy frequency [%]
100
80
60
40
20
0
+/+
+/-
-/-
n = 61
n = 63
n = 51

Fig. 1

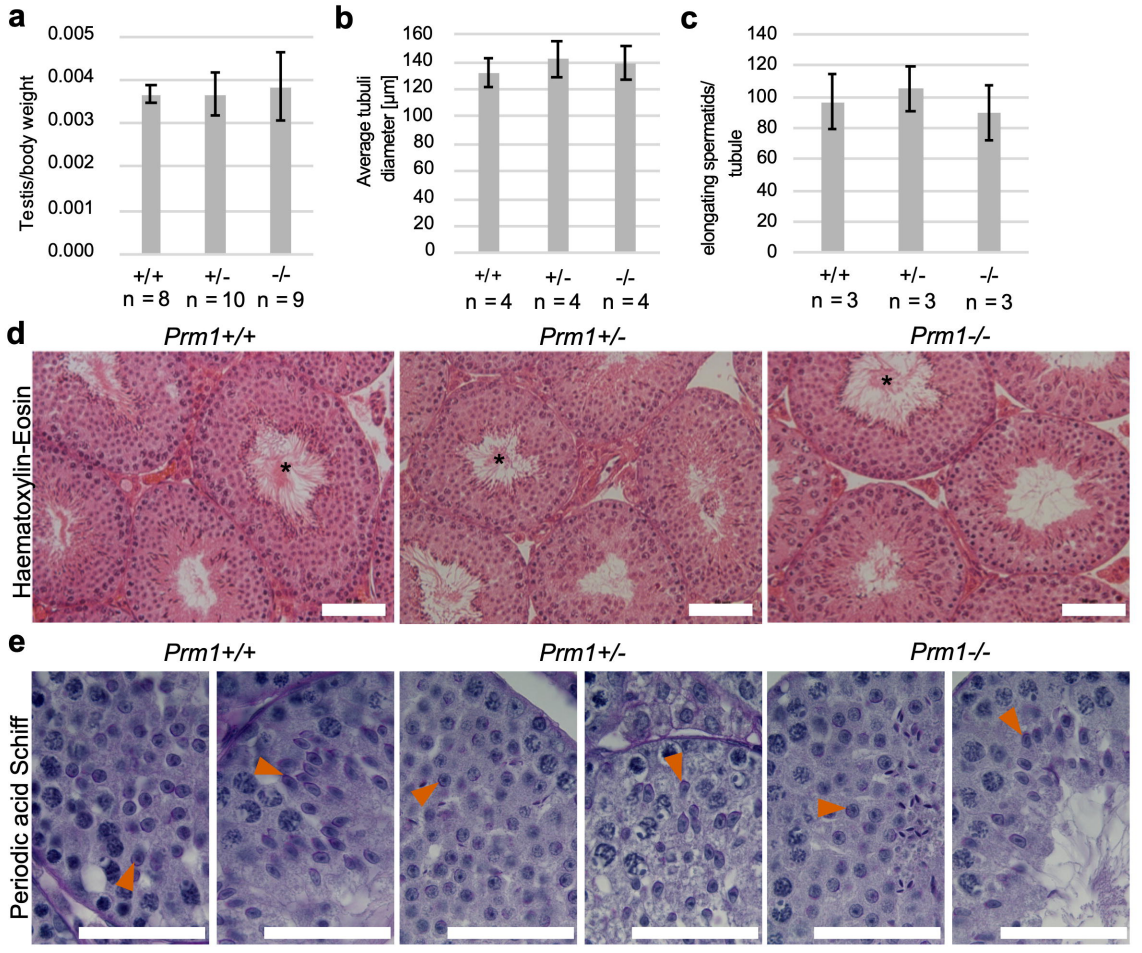
a
Testis/body weight
0.005
0.004
0.003
0.002
0.001
0.000
+/+ n = 8
+/- n = 10
-/- n = 9
b
Average tubuli diameter [µm]
160
140
120
100
80
60
40
20
0
+/+ n = 4
+/- n = 4
-/- n = 4
c
elongating spermatids/ tubule
140
120
100
80
60
40
20
0
+/+ n = 3
+/- n = 3
-/- n = 3
d
Prm1+/+
Prm1+/-
Prm1-/-
Haematoxylin-Eosin
e
Prm1+/+
Prm1+/-
Prm1-/-
Periodic acid Schiff

Fig. 2

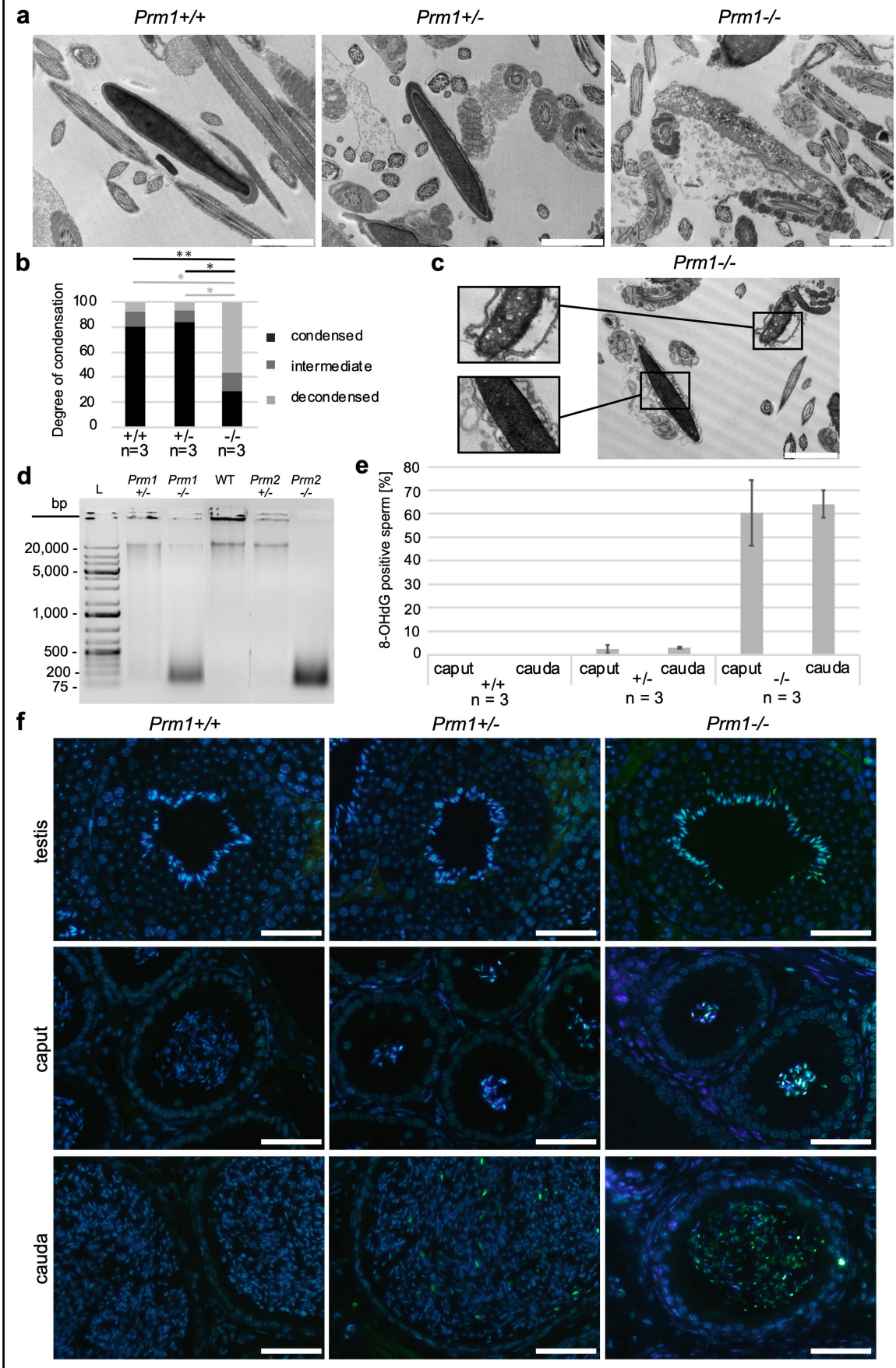
a
Prm1+/+
Prm1+/-
Prm1-/-
b
Degree of condensation
100
80
60
40
20
0
+/+ n=3
+/- n=3
-/- n=3
condensed
intermediate
decondensed
c
Prm1-/-
d
L
Prm1 +/-
Prm1 -/-
WT
Prm2 +/-
Prm2 -/-
bp
20,000
5,000
1,000
500
200
75
e
8-OHdG positive sperm [%]
80
70
60
50
40
30
20
10
0
caput
cauda
+/+ n = 3
+/- n = 3
-/- n = 3
f
Prm1+/+
Prm1+/-
Prm1-/-
testis
caput
cauda

Fig. 3

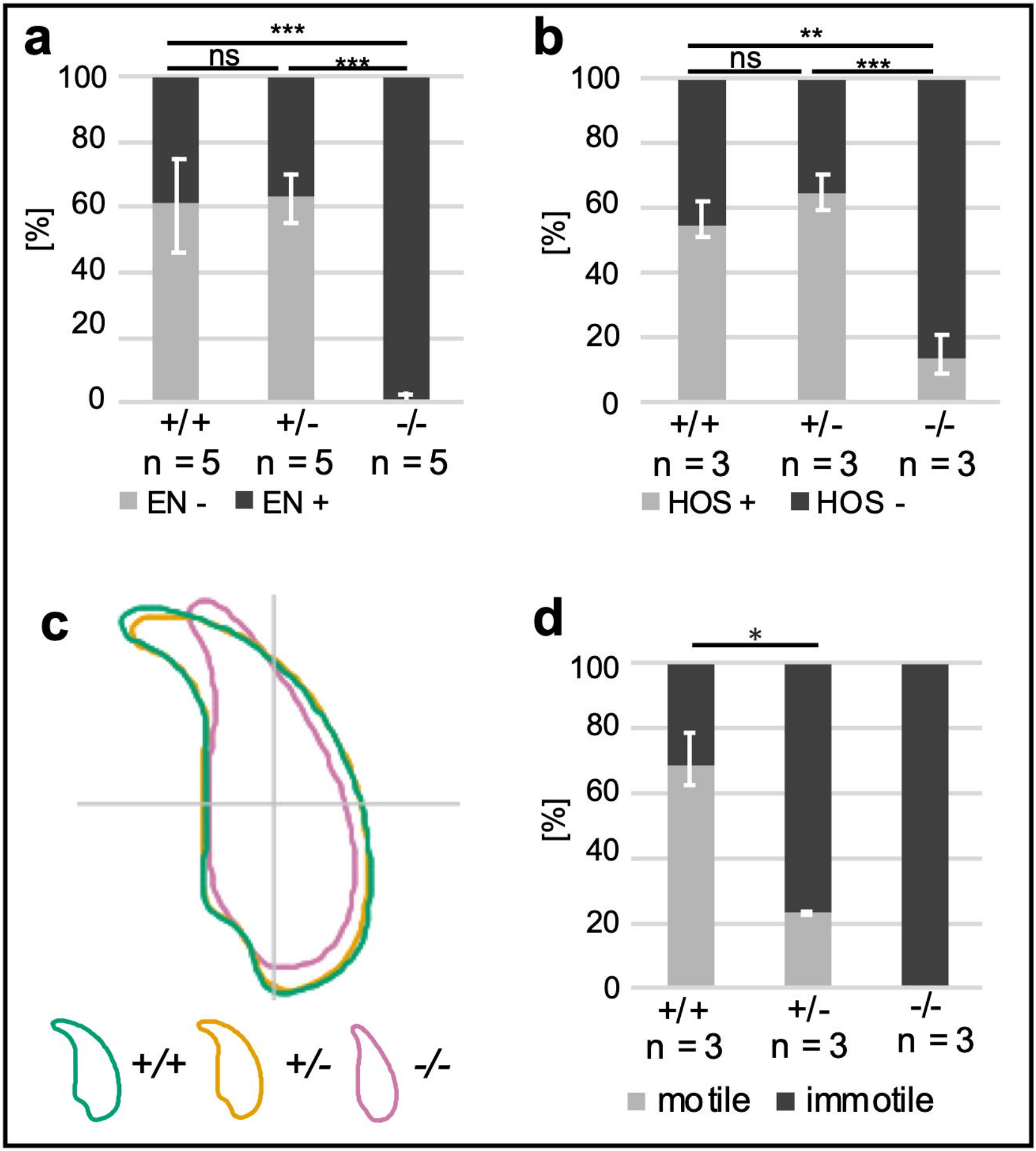
a
***
ns
***
100
80
60
40
20
0
[%]
+/+
+/-
-/-
n = 5
n = 5
n = 5
EN -
EN +
b
**
ns
***
100
80
60
40
20
0
[%]
+/+
+/-
-/-
n = 3
n = 3
n = 3
HOS +
HOS -
c
+/+
+/-
-/-
d
*
100
80
60
40
20
0
[%]
+/+
+/-
-/-
n = 3
n = 3
n = 3
motile
immotile

Fig. 4

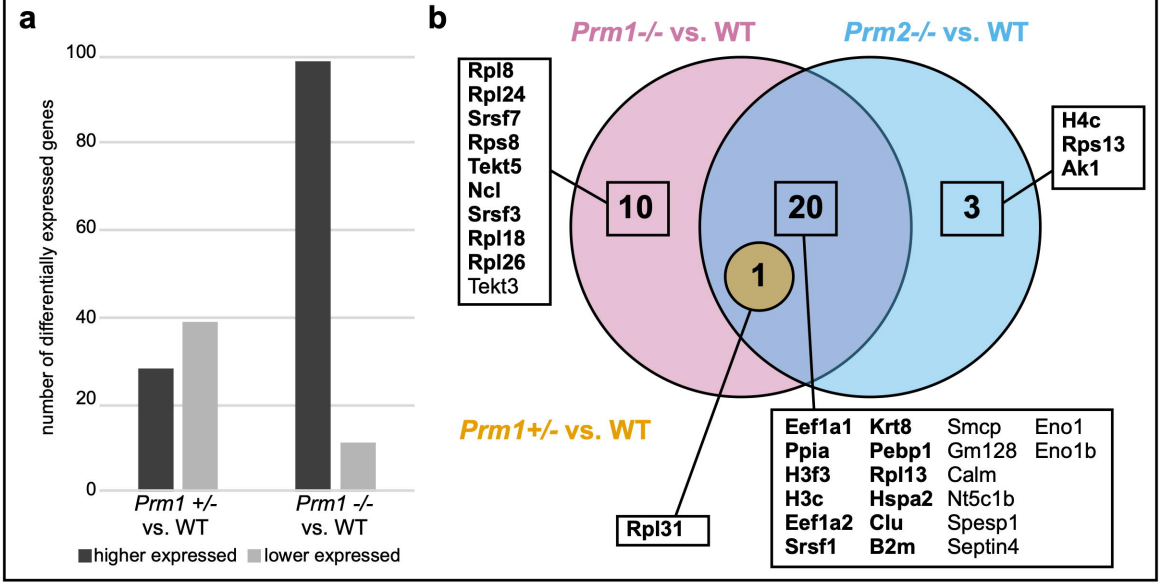
a
number of differentially expressed genes
100
80
60
40
20
0
Prm1 +/- vs. WT
Prm1 -/- vs. WT
higher expressed
lower expressed
b
Prm1-/- vs. WT
Prm2-/- vs. WT
Prm1+/- vs. WT
Rpl8
Rpl24
Srsf7
Rps8
Tekt5
Ncl
Srsf3
Rpl18
Rpl26
Tekt3
10
20
3
1
H4c
Rps13
Ak1
Rpl31
Eef1a1 Krt8 Smcp Eno1
Ppia Pebp1 Gm128 Eno1b
H3f3 Rpl13 Calm
H3c Hspa2 Nt5c1b
Eef1a2 Clu Spesp1
Srsf1 B2m Septin4

Fig. 5

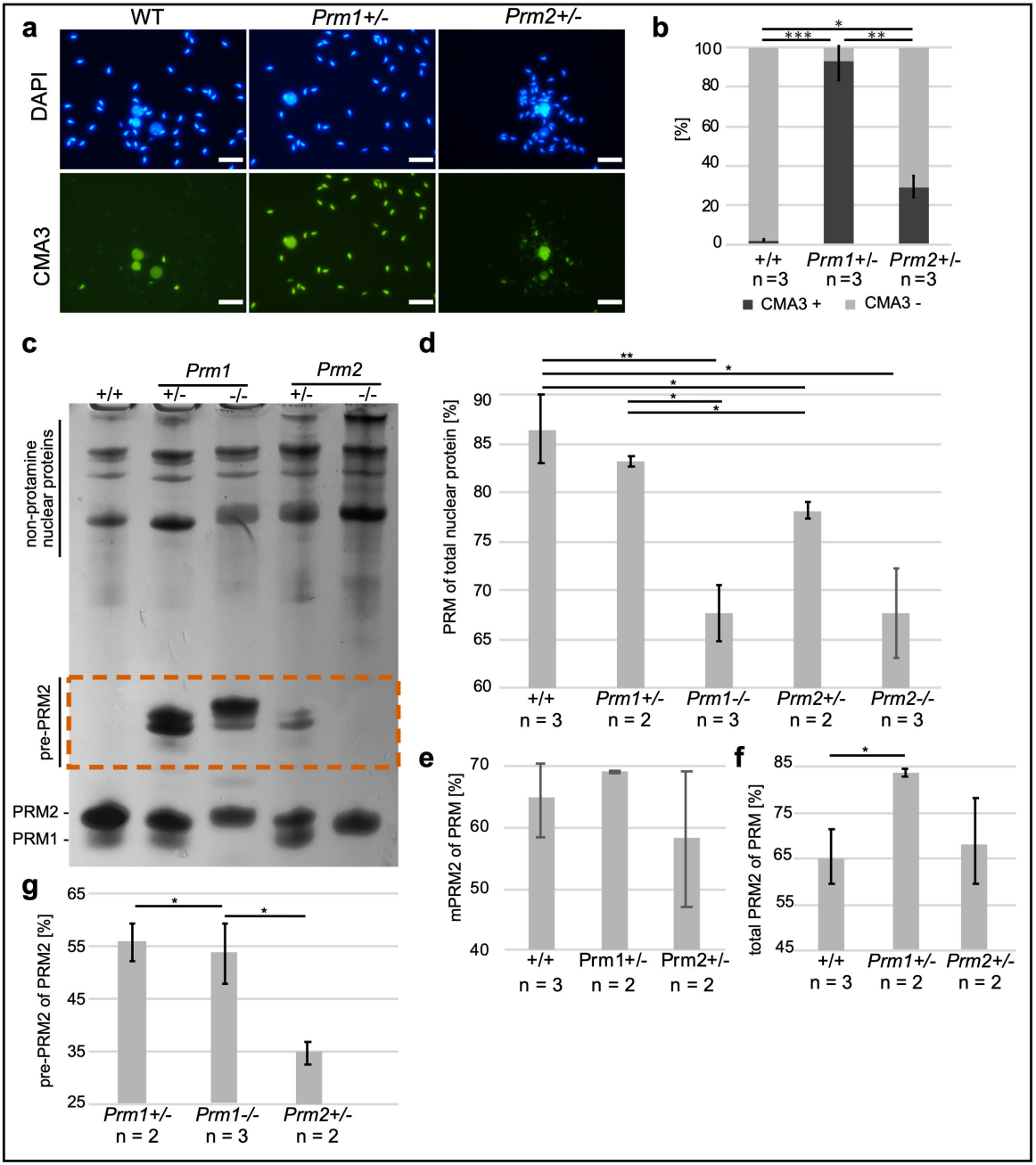
a
WT
Prm1+/-
Prm2+/-
DAPI
CMA3
b
[%]
100
80
60
40
20
0
*
***
**
+/+ n=3
Prm1+/- n=3
Prm2+/- n=3
CMA3 +
CMA3 -
c
Prm1
Prm2
+/+
+/-
-/-
+/-
-/-
non-protamine nuclear proteins
pre-PRM2
PRM2 -
PRM1 -
d
PRM of total nuclear protein [%]
90
85
80
75
70
65
60
+/+ n = 3
Prm1+/- n = 2
Prm1-/- n = 3
Prm2+/- n = 2
Prm2-/- n = 3
e
mPRM2 of PRM [%]
70
60
50
40
+/+ n = 3
Prm1+/- n = 2
Prm2+/- n = 2
f
total PRM2 of PRM [%]
85
75
65
55
45
+/+ n = 3
Prm1+/- n = 2
Prm2+/- n = 2
g
pre-PRM2 of PRM2 [%]
65
55
45
35
25
Prm1+/- n = 2
Prm1-/- n = 3
Prm2+/- n = 2

Fig. 6